Mutagenesis Mapping of RNA Structures within the Foot-and-Mouth Disease Virus Genome Reveals Functional Elements Localised in the Polymerase ($3D^{pol}$) Encoding Region.

Lidia Lasecka-Dykes[a,¥,#], Fiona Tulloch[b,¥,*], Peter Simmonds[c], Garry A. Luke[b], Paolo Ribeca[a,*], Sarah Gold[a], Nick J. Knowles[a], Caroline F. Wright[a], Jemma Wadsworth[a], Mehreen Azhar[a], Donald P. King[a], Tobias J. Tuthill[a], Terry Jackson[a], Martin D. Ryan[b,#]

[a]The Pirbright Institute, Pirbright, Surrey, United Kingdom.

[b]Biomedical Sciences Research Complex (BSRC), School of Biology, University of St. Andrews, St. Andrews, United Kingdom.

[c]Nuffield Department of Experimental Medicine, University of Oxford, Oxford, United Kingdom.

Running Head: Novel functional RNA structures within the FMDV genome

#Address correspondence to Lidia Lasecka-Dykes, lidia.dykes@pirbright.ac.uk and Martin D. Ryan, mdr1@st-andrews.ac.uk

*Present address: Fiona Tulloch, Benchmark Animal Health, Edinburgh, Scotland, United Kingdom; Paolo Ribeca, Biomathematics and Statistics Scotland, Edinburgh, Scotland, United Kingdom.

20 ¥Lidia Lasecka-Dykes and Fiona Tulloch contributed equally to this work. Author order

21 was agreed upon by all authors.

22

23 Abstract: 250 words

24 Importance: 150 words

25 Text: 4,589 words

ABSTRACT

Abstract: RNA structure plays a crucial role in the replication of positive sense RNA viruses and can form functional elements within the untranslated regions (UTRs) and the protein coding sequences (or open reading frames (ORFs)). While RNA structures in the UTRs of several picornaviruses have been functionally characterised, the roles of putative RNA structures predicted for the ORF remain largely undefined. Here we have undertaken a bioinformatic analysis of the foot-and-mouth disease virus (FMDV) genome and predicted the existence of 53 evolutionarily conserved RNA structures within the ORF. Forty-five (45) of these structures were located in the regions encoding the non-structural proteins (nsps). To investigate if the structures in the regions encoding the nsps are required for FMDV replication we used a mutagenesis method, CDLR mapping, where sequential coding segments were shuffled to minimise RNA secondary structures while preserving protein coding, native dinucleotide frequencies and codon usage. To examine the impact of these changes on replicative fitness, mutated sequences were inserted into an FMDV sub-genomic replicon. We found that three of the RNA structures, all at the 3' termini of the FMDV ORF, were critical for replicon replication. Contrastingly, disruption of the other 42 conserved RNA structures that lie within the regions encoding the nsps had no effect on replicon replication, suggesting that these structures are not required for initiating translation or replication of viral RNA. Conserved RNA structures that are not essential for virus replication could provide ideal targets for the rational attenuation of a wide range of FMDV strains.

Importance: Some RNA structures formed by the genomes of RNA viruses are critical for viral replication. Our study shows that of 45 conserved RNA structures located within

the regions of the foot-and-mouth disease virus (FMDV) genome that encode the non-structural proteins, only three are essential for replication of an FMDV sub-genomic replicon. Replicons replication is dependent on RNA translation and synthesis; thus, our results suggest that the three RNA structures are critical for either initiation of viral RNA translation and/or viral RNA synthesis. Although further studies are required to identify if the remaining 42 RNA structures have other roles in virus replication, they may provide targets for the rational large-scale attenuation of a wide range of FMDV strains. FMDV causes a highly contagious disease posing a constant threat to global livestock industries. Such weakened FMDV strains could be investigated as live-attenuated vaccines or could enhance biosecurity of conventional inactivated vaccine production.

INTRODUCTION

The genomes of RNA viruses not only encode proteins but also contain non-templated functional elements in both the coding and untranslated regions (UTRs). These can be secondary or higher order RNA structures such as simple stem-loops or more complex structures which include pseudoknots and so-called kissing-loops that mediate long-range RNA-RNA interactions (1-12) . The function, shape and number of such RNA functional elements is often characteristic for a particular group of viruses, where they play important roles in processes such as the initiation of viral RNA translation and replication, subgenomic mRNA transcription, frame shift events, viral RNA encapsidation and modulation of host's antiviral responses (reviewed in (13)). Since many RNA viruses are of medical and veterinary importance, characterisation of these RNA structures brings us closer to understanding viral pathogenicity and provides opportunities for disease control.

Foot-and-mouth disease virus (FMDV) is the causative agent of foot-and-mouth disease (FMD), a highly contagious disease of cloven-hoofed animals (including livestock) (reviewed in (14)). FMD is endemic in Africa and Asia, where it impacts upon productivity and trade as well as posing a constant threat of causing costly incursions into disease-free countries (15-21). Control of FMD by vaccination in endemic settings is complicated by the high antigenic variability of the seven serotypes of FMDV: A, Asia 1, C (not reported since 2004), O, Southern African Territories (SAT) 1, SAT 2 and SAT 3 (19, 20, 22-24).

FMDV is a small non-enveloped positive-sense single-stranded RNA virus classified in the species *Foot-and-mouth disease virus*, genus *Aphthovirus* in the family *Picornaviridae*. The FMDV genome is ~ 8.5 Kb in size and composes of a single, long open reading frame (ORF) which is flanked by 5' and 3' UTRs (reviewed in (25)). The encoded polyprotein is co- and post-translationally cleaved by viral proteases (L^{pro} and $3C^{pro}$) and by a ribosomal skipping event mediated by the 2A peptide into a number of functional precursors and the mature proteins (26-34). The coding sequence for the FMDV ORF is arbitrarily divided into four regions (5'-L^{pro}, P1, P2 and P3-3'). The P1 region encodes the capsid proteins (1A, 1B, 1C and 1D, also called VP4, VP2, VP3 and VP1, respectively), while the P2 and P3 regions encode the non-structural proteins (nsps) (reviewed in (25)).

There are a number of RNA structures within picornavirus genomes that have been accurately predicted and characterised biochemically (12, 35-39). These structures are predominantly located in the UTRs and have been shown to be important for replication and translation of picornavirus genomes (reviewed in (40)). Within the 5' UTR of the FMDV genome, the S-fragment forms a single, long hairpin structure (293-381 nucleotides (nts) in length) and has been reported to play a role in viral replication and innate immune modulation (41-45). Elsewhere in the 5' UTR, the presence of multiple (2 - 4) pseudoknots downstream of the poly(C) tract has been shown to determine virus tropism (41, 46). Other key and well-characterised RNA structural elements include a type II internal ribosome entry site (IRES), which initiates cap-independent translation of the viral genome (41, 47-50); while the *cis*-acting replication element (*cre*) acts as a template for uridylylation of the VPg (3B) protein, which then

105 acts as a primer for synthesis of viral RNA (51, 52). The 3' UTR of the FMDV genome is
106 located upstream of the poly(A) tract and contains two RNA stem-loop structures called
107 SL1 and SL2. These stem-loops interact non-simultaneously with the S-fragment and
108 IRES forming long-range interactions that have been shown to be necessary for viral
109 RNA replication (43, 53, 54).

110 A number of other secondary RNA structures have been predicted
111 computationally to be present within the FMDV ORF (12). However, with the exception
112 of packaging signals (55), the role(s) of these structures in the FMDV replication cycle
113 have not been determined. In this study we have identified 45 evolutionarily conserved
114 RNA structures within the regions of the FMDV ORF that encode for the nsps.
115 Mutagenesis of these structures identified three novel RNA stem-loops in the coding
116 region of the RNA-dependent RNA polymerase ($3D^{pol}$) that are essential for replication
117 of an FMDV sub-genomic replicon, suggesting that these structures are required for
118 either initiation of viral RNA translation and/or viral RNA synthesis. In contrast,
119 mutagenesis of the remaining 42 structures had no effect on replicon replication. This
120 approach can aid in the identification of critical viral RNA structures required for viral
121 genome replication, and also help identify conserved RNA structures that are not
122 essential for virus replication that could provide ideal targets for the rational attenuation
123 of a wide range of FMDV strains.

124 **RESULTS**

125 **Prediction of conserved RNA structures within the FMDV genome.** While
126 previous studies have provided evidence that the FMDV genome is highly structured

with conserved RNA base pairing throughout the coding part of the genome (12, 56), these studies were conducted on a relatively small dataset. Since the number of full genome sequences available on public databases has greatly increased in recent years, before conducting functional studies, we revisited these analyses to predict conserved RNA stem-loops that were common in 118 representative genomic sequences covering all FMDV serotypes (see materials and methods section for isolates information).

Firstly, average mean folding energy differences (MFED) across whole FMDV genomes were determined for all viral isolates used in this study. In this method, conserved minimum free energy (MFE) values were normalised to MFE values of native sequences that had been scrambled using an NDR algorithm, which preserves the dinucleotide frequencies of native sequences. This ensures that reported values are not purely due to G+C or other composition biases (see material and methods for detail) (57-59). In order to show distribution of the MFED values along the genome, this analysis employs an incremental sliding window computation with user-defined window size and increment (60) (in our case 400 and 20 nts, respectively, where each 400 nts segment overlapped its neighbours by 380 nts). A 400 nts window allowed for detection of the S-fragment structure, while ignoring potential long-distance RNA-RNA interactions for which biological significance is hard to verify. Despite the high genomic sequence diversity across all seven serotypes (20% mean nucleotide pairwise distance (± 9% standard deviation (StDev)), with 31% (± 5% StDev) and 14% (± 7% StDev) average pairwise distance in the regions encoding the capsid proteins and the nsps, respectively), all the FMDV genomes analysed showed high folding energies across most of their sequence compared to the permuted controls (Fig. 1). This indicates that

all FMDV sequences possess a similar extent of sequence order-dependent RNA secondary structure. To confirm this, full genome sequences were grouped into those of Eurasian (A, Asia 1, C and O serotypes) and SAT (SAT 1 - 3 serotypes) origin and average MFED values were determined along the genome for each group. Although we recognize that the grouping may not completely accommodate the inter-serotypic history of these viruses (see (45) for details why grouping viruses into SAT and non-SAT clusters is not always correct), the MFED plots showed similar patterns of high and low MFED values across the genome. MFED values were better correlated between FMDV groups in the UTRs and the regions encoding the nsps identifying a potentially greater degree of RNA structure conservation compared to the more genetically divergent region encoding the capsid proteins (Fig. 1).

The window size used for MFED scanning does not identify individual RNA structures and only highlights regions with high folding energies (which may contain dissimilar structures and/or structures located at different positions). Therefore, RNAalifold program, implemented in The ViennaRNA Package (61), was used to identify individual conserved RNA stem-loops for the 118 whole genomic sequences and for individual FMDV serotypes. Stem-loops that were conserved in all seven serotypes were visualised as a dot plot graph, plotting each nucleotide pairing (represented by individual dot) against positions of involved nucleotides on the x and y axes (Fig. 1). Any pairing interactions distanced by more than 400 nts were removed post analysis. By excluding long-distance interactions post whole genome RNA structure prediction, we did not ignore the effect they may have on formation of local

pairings. RNAalifold cannot predict pseudoknots, and therefore the region directly downstream of the poly(C) tract was excluded from our analyses (Fig. 1).

These analyses correctly predicted the presence of well-characterised RNA secondary structures in the FMDV genome: the S-fragment, IRES and *cre*, all located in the 5' UTR, and SL1 and SL2 located in the 3' UTR (Fig. 1 and Fig. S1). It additionally identified several serotype-specific conserved stem-loops in the region encoding the capsid proteins, but only four of these were conserved in all seven serotypes. In contrast, 45 stem-loops (when counting each RNA hairpin individually, even within a single branched structure) were universally present within the regions encoding the nsps (Fig. 1, Table 1). Overall, there were 53 highly conserved stem-loops in the ORF of the FMDV genome that were conserved across all serotypes (Table 1).

Use of CDLR mutagenesis for functional mapping of predicted RNA structures. Next, we undertook mutagenesis studies to investigate whether any of the conserved RNA structures identified in the FMDV genome play a functional role in viral replication. FMDV replicons lack the region encoding the capsid proteins but are replication competent, demonstrating that there are no RNA elements essential for translation or replication of viral RNA within the capsid encoding region. Therefore, our investigation focused on structures located within the regions encoding the nsps of the replicon. Additionally, the effect on replication of changes incorporated into the replicon can be analysed in real-time through monitoring of fluorescence from an integrated green fluorescent protein (GFP) reporter gene that replaced the region encoding the capsid proteins (62).

194 In order to mutate the conserved RNA structures predicted within the regions
195 encoding the nsps while maintaining codon composition, codon order and dinucleotide
196 frequencies of the native WT replicon sequence we applied CDLR scrambling method
197 (11, 56). To monitor its effectiveness in altering or otherwise disrupting RNA pairing
198 within the native sequence, sequence of the regions encoding the nsps of WT replicon
199 was randomly permutated 50 times using the CDLR algorithm. Then, MFED values for
200 these mutants were calculated as described above and these were compared to MFED
201 values of the native WT replicon sequence and the corresponding sequences of the 118
202 FMDV isolates used in this study. Sequences generated by CDLR showed evidence of
203 severely disrupted RNA secondary structures, with a mean MFED value of 2.2% (StDev
204 ±1.4%), compared to a mean value of 10.9% (StDev ±1.2%) for the corresponding
205 regions of the native FMDV sequences and that of the WT FMDV replicon (Fig. 2).

206 To identify functional RNA structures, we divided the regions encoding the nsps
207 of the WT replicon (ptGFP-replicon) into nine consecutive fragments defined by unique
208 restriction sites, and individually permutated each fragment using the CDLR algorithm
209 (Fig. 3A-B). To further verify the extent of changes to the RNA structure introduced by
210 the CDLR algorithm, we used the RNAforester program implemented in The
211 ViennaRNA Package (61, 63, 64). This compared the putative structures adopted by the
212 CDLR-permuted regions (shown in Fig. 3A-B) to the structures located within the
213 corresponding regions of the WT replicon sequence. RNAforester calculates RNA
214 secondary structure alignments based on the tree alignment model and quantifies
215 similarity of structures in question, where the relative similarity score values equal to
216 one represent two identical structures (61, 63, 64). With the exception of the 2C

encoding region, which exhibits some structure similarity between CDLR and WT replicon (Fig. S2), there was low structural similarity between equivalent WT and CDLR genomic fragments (Table 2). RNA structures located in the 5' and 3' UTRs were generally unaffected by any CDLR permutation of the adjacent or more distal regions encoding the nsps, with the exception of the SL1 stem-loop in the 3' UTR that was shorter by 11 pairings (Fig. S3).

CDLR replicon mutants reveal regions of secondary structure required for replication of an FMDV replicon. Next, we examined the effect of RNA structure disruption on replication of the FMDV replicon using mutant replicons containing CDLR-permuted sequences over different parts of the regions encoding the nsps. For this we used two different continuous cell lines known to support FMDV replication (Fig. 3A-B). The replication kinetics of the mutant replicons was compared to the WT ptGFP-replicon and a replicon with an inactive polymerase (ptGFP-3D^{pol}GNN, previously described in (65)). Since replication levels at 8 hours post-transfection (hpt) were representative of the entire experiment (Fig. S4), for simplicity, data for this time point are shown. In both cell lines (BHK-21 and MDBK, of hamster and bovine origin, respectively), all of the CDLR mutant replicons tested displayed replication kinetics comparable to the WT ptGFP-replicon except for the replicon which carried a mutated sequence within the 3' terminal part of the 3D^{pol} encoding region (called 3D$_3$, Fig. 3C). The replicon with 3D$_3$ mutated encoding region was replication defective in both cell lines, with replication levels equivalent to the negative control replicon (ptGFP-3D^{pol}GNN; Fig. 3C). These results strongly suggest that this part of the 3D^{pol} encoding region contains RNA structures crucial for replication of the FMDV replicon. Consistent with their inferred

location in $3D_3$, CDLR permutation of the entire Δ1D-3A and 3A-$3D_2$ encoding region showed little effect on the replication kinetics (Fig. S5).

Modification of individual stem-loops within the $3D_3$ region impairs replication of an FMDV replicon. Our results indicate that the region of the FMDV genome encoding for the 3' terminal end of $3D^{pol}$ (called here $3D_3$) contains conserved secondary RNA structures that may be necessary for replication of the FMDV replicon. Therefore, the RNA structures present in this region were investigated in more detail by visualising each individual structure and comparing it to the corresponding scrambled region within the CDLR mutant. Analysis of corresponding sequences of FMDV field isolates (over the $3D_3$ region) revealed five stem-loops (SL7 – SL11) with strong nucleotide pairing conservation, with SL10 being the most conserved structure (Fig. 4A). Variability within all structures was accommodated though the occurrence of covariant changes that preserved nucleotide pairings (Fig. 4A). Additionally, there was substantial nucleotide sequence conservation in the sequence forming the unpaired loop at the top of the stem-loop structures (i.e., in the hairpin loops) of SL7, SL8 and SL9 (Fig. 5) implying some functional constraints on these sequences. Each of the predicted structures in the WT sequence were substantially disrupted in the CDLR scrambled mutant (Fig. 4B).

Further studies were therefore undertaken to dissect the importance of the individual stem-loops within the $3D_3$ fragment for replication of the FMDV replicon. Each of the five putative RNA structures in the $3D_3$ region of the WT replicon were permuted individually *in silico* introducing the maximum number of nucleotide changes possible to disrupt the RNA structure whilst maintaining amino acid coding, dinucleotide

frequencies and the integrity of the neighbouring RNA structures (Fig. 6 and 7A). Additionally, a replicon where all five putative RNA stem-loops were altered (SL7-11^{mut}, using the same mutation strategy as for each individual loop, Fig. 7A) acted as a negative control (in addition to the replicon with CDLR-scrambled 3D$_3$ region) to confirm that mutation of these particular stem-loops, and not of other elements present in the CDLR replicon with the permutated 3D$_3$ region, impaired RNA replication. Replication of ptGFP-replicons carrying individual mutated stem-loops was tested in the same two cell lines as described above (Fig. 7). As previously observed, replication levels at 8 hpt were representative of the replication kinetics (Fig. S6). Replication of replicons with disrupted SL7 and SL8 was not affected in either cell line (Fig. 7B). In contrast, replication of replicons with disrupted SL9 or SL10 were significantly reduced, although the effect on replication varied between the cell lines. Disruption of SL9 led to only a marginal, but statistically significant, reduction of replication in BHK-21 cells (GFP intensity equal 94% of the GFP signal of the WT replicon, p-value=0.02), whereas the negative effect on replication in MDBK cells was greater (GFP intensity equal 49% of the GFP signal of the WT replicon, p-value < 0.001). In both cell lines, disruption of SL10 reduced replication to a greater extent than disruption of SL9 (GFP intensity, 52% (p-value < 0.001) of the GFP signal of the WT replicon in BHK-21 cells, and 24% (p-value < 0.001) of the GFP signal of the WT replicon in MDBK cells), with the replication profile in bovine cells being close to the replicon with an inactive polymerase (ptGFP-3D^{pol}GNN) and the replicon with the 3D$_3$ region mutated by the CDLR algorithm (Fig. 7B). Replication of the replicon with disrupted SL11 was reduced only in MDBK cells (GFP intensity equal 85% of the GFP signal of the WT replicon, p-value < 0.001), but not BHK-21 cells. Finally, the replicon with all five stem-loops altered (SL7-11^{mut})

287 demonstrated replication comparable to the ptGFP-3D^{pol}GNN replication-deficient
288 control (which give a GFP signal due to translation of the input RNA) in both cell lines
289 tested (~20% of WT GFP signal, p-value < 0.001, Fig. 7B).

290 To investigate whether the combined mutagenesis of SL9, SL10 and SL11 has a
291 detrimental effect on replication of the FMDV replicon, constructs with two loops
292 disrupted (SL9,10^{mut} and SL9,11^{mut}), or all three loops disrupted (SL9-11^{mut}) were tested
293 as described above for the individual stem-loop mutations (Fig. 8A). In both cell lines,
294 disruption of SL9 in combination with SL10 (SL9,10^{mut}) resulted in a marked reduction of
295 replicon replication when compared to replicons with the SL9 and SL10 mutated
296 individually (see Fig. 7B and 8B). Replication of the SL9,10^{mut} replicon was severely
297 disrupted (GFP intensity equal 27% (p-value < 0.001) and GFP intensity equal 20% (p-
298 value < 0.001) of the GFP signal of the WT replicon in BHK-21 and MDBK cells,
299 respectively), with replication levels comparable to the SL7-11^{mut} negative control (Fig.
300 8B). Interestingly, disruption of SL11 in combination with SL9 (SL9,11^{mut}) resulted in a
301 significant reduction of replicon replication in both cell lines (GFP intensity equal 60%
302 (p-value < 0.001) and GFP intensity equal 36% (p-value < 0.001) of the GFP signal of
303 the WT replicon in BHK-21 and MDBK cells, respectively; Fig. 8), although in BHK-21
304 cells individual mutation of SL9 and SL11 had only a marginal or no effect, respectively
305 (see Fig. 7). Our computational prediction of SL9,11^{mut} did not suggest any disruption of
306 the SL10 secondary structure, which is indirectly confirmed by the experimental data
307 where replication impairment caused by joint permutation within SL9,11^{mut} is
308 significantly less than that of the SL9-11^{mut} (GFP intensity equal 60% (p-value < 0.001)
309 vs GFP intensity equal 28% (p-value < 0.001) of the GFP signal of the WT replicon in

BHK cells, and GFP intensity equal 36% (p-value < 0.001) vs GFP intensity equal 20% (p-value <0.001) of the GFP signal of the WT replicon in MDBK cells, Fig. 8B). In both cell lines tested, disruption of all three stem-loops (SL9-11^{mut}) resulted in a replication profile comparable to the SL7-11^{mut} (Fig. 8B). Table 3 summarises effect of mutagenesis of each of these stem-loops (individually and in combination) on replication of the FMDV replicon.

Comparison of the conserved stem-loops within the FMDV 3D$_3$ region to structures found in the 3' terminal 3D encoding region of poliovirus. Two stem loops (referred to as loop α and β in Song *et al.* 2012) necessary for poliovirus (PV) replication are present in the 3' terminal encoding sequence of PV 3D^{pol} (37, 38). Since PV is a member of a different genus in the family *Picornaviridae* and distantly related to FMDV, we investigated whether any of the stem-loop structures found in the 3' end of the 3D^{pol} encoding region of the FMDV genome were similar to those present in the equivalent part of the PV genome. Therefore, we compared each of the FMDV RNA structures (SL7 to SL11) to the PV loops α and β using RNAforester. As described in Table 4, the structures identified in the 3' terminal part of the coding region of FMDV 3D^{pol} do not appear to resemble those found in the equivalent position of the PV genome, while (using the same approach) the *cre* structures of PV and FMDV showed some structural similarity.

DISCUSSION

Many aspects of FMDV replication remain poorly understood, such as the function of RNA structures found within the ORF. Here we revisited the RNA structural

332 architecture of the FMDV genome and, for the first time, investigated whether the
333 putative stem-loops localised within the ORF are required for viral genome replication.
334 Our results are in line with previous studies showing that FMDV has extensive RNA
335 structure throughout the genome, substantially exceeding that found in viruses of other
336 genera of the family *Picornaviridae* (e.g. MFED value >10% for FMDV genomic
337 sequences comparing to <4% for viral sequences belonging to genus *Enterovirus*,
338 *Hepatovirus*, *Parechovirus* and *Teschovirus*) (12, 56, 59). When compared to the
339 previous structure predictions performed by Witwer *et al.* 2001, our study identified a
340 greater number of conserved RNA structures within the FMDV ORF (53 stem-loops,
341 with some merging into 46 branched structures, versus 25 structures predicted
342 previously). Since we used a larger dataset than the previous authors (118 relatively
343 diverse FMDV sequences versus nine used by Witwer *et al.* 2001), it is possible that we
344 obtained a stronger statistical signal supporting conservation of these additional
345 structures. Importantly, we found that three of the structures within the coding region of
346 $3D^{pol}$ (i.e., SL9, SL10 and SL11) are critical for efficient replication of an FMDV replicon,
347 thereby implying that they would provide the same function during virus replication.

348 Despite consistently elevated MFED values, the FMDV capsid encoding region
349 contained only four RNA stem-loops which were conserved in all serotypes. Viral
350 genomes characterised by high MFED values and low conservation of individual RNA
351 structures have been observed before (66). For instance, the coding region of hepatitis
352 C virus (HCV) showed elevated MFED values, while, except for the terminal genomic
353 regions, the individual stem-loop structures were distinct between different HCV
354 genotypes and even subtypes (66-68). Similarly, FMDV showed dense serotype-specific

355 RNA structure within its capsid encoding region, which were not shared among other
356 serotypes (as found in (66) and independently in here).

357 To identify functional RNA structures, we applied the CDLR algorithm to permute
358 a genomic FMDV sequence (60). While the degree of possible mutagenesis is
359 necessarily limited by protein coding, dinucleotide frequency, and codon usage
360 constraints, the CDLR algorithm substantially disrupted secondary RNA structure of the
361 native FMDV sequence in all regions apart from region encoding for 2C (Table 2 and
362 Fig. S2). Since the permutation of the entire Δ1D-3A encoding region (which resulted in
363 more extensive changes to the RNA structure) had a minimal effect on replication of the
364 FMDV replicon, it is safe to state that conserved RNA stem-loops within the 2C
365 encoding region are not essential for replicon of the FMDV replication *in vitro*.

366 Contrastingly, the CDLR scanning method identified three structures located at
367 the 3' terminal part of the $3D^{pol}$ encoding region that were important for replication of the
368 FMDV replicon. Of these, SL10 showed the highest degree of pairing conservation and
369 appeared to be the predominant structure important for replication of the FMDV
370 replicon. Mutation of SL9, SL10 or SL11 showed a much greater reduction of replicon
371 replication in MDBK cells compared to BHK cells. MDBK cells have been shown to
372 secrete high levels of interferon (IFN) upon stimulation (69), while BHK-21 cells are
373 known to lack an intact IFN pathway (70, 71). Furthermore, a number of published
374 results suggest that RNA structure might directly or indirectly play a role in the
375 modulation of antiviral responses (42, 54, 72, 73). Collectively, these observations
376 suggest that SL9, SL10 and SL11 could play additional roles in the evasion of antiviral
377 responses, and therefore mutation of these structures led to a drastic reduction in

replication of the FMDV replicon in IFN-competent cell lines. In both cell lines tested, deletion of two or more stem-loops (SL9, SL10 and SL11) in combination significantly impaired replication of the replicon, suggesting that even in the absence of a fully functional antiviral pathway all three stem-loops are important for FMDV replication. Similarly to the viral genome, replication of an FMDV replicon involves viral protein synthesis, and the sequential synthesis of negative- (i.e. complementary) and positive-strand (i.e. genomic) viral RNA. Thus, although SL9-11 are required for replication of the replicon further studies are required to dissect which of these process (viral RNA translation and/or viral RNA replication) are dependent on SL9, SL10 and SL11. Interestingly, in the PV genome stem-loops within the coding region of $3D^{pol}$ have been identified that are requited for viral RNA synthesis (37, 38). However, these structures do not appear to share sequence or structural similarity with SL9, SL10 or SL11 in the FMDV genome.

The observation that replication of the FMDV replicon mutants with disrupted RNA structure elsewhere in the regions encoding the nsps (i.e., spanning 1D through to most of $3D^{pol}$) was surprising. The maintenance of extensive conserved internal base-pairing and consistently elevated MFED values observed in the relatively diverse set of FMDV isolate sequences analysed indeed strongly argues that the RNA structures formed by those genomic regions must play some functional role in the FMDV replication cycle. It is possible that at least some of the apparently 'non-functional' RNA structures are genome-scale ordered RNA structure (GORS) which may play a role in persistence of FMDV in its natural host (56, 59). While FMDV causes an acute disease in domestic animals (14, 74), it is known to persist in African Buffalo (*Syncerus caffer*),

401 which are a natural reservoir of the virus (75-78). Since FMDV and African Buffalo are
402 thought to have co-evolved together, it is possible that GORS developed in the FMDV
403 genome as a part of the virus-host co-adaptation, where they might assist in evasion of
404 immune recognition. The link between GORS, persistence and ability to minimise
405 antiviral sensing has been shown for number of unrelated viruses (56, 59, 66, 72). Work
406 is currently underway to investigate whether any of these remaining structures play a
407 role in modulation of the antiviral sensing during FMDV replication in its natural host
408 environment.

409 Although the function of the apparently non-essential RNA structures within the
410 regions encoding the nsps remains to be defined, due to their conserved nature, they
411 form a potential target for genome-scale attenuation of a wide range of FMDV strains.
412 Such a strategy could contribute to the development of live attenuated FMD vaccines
413 that may improve on the short duration of immunity, which is a shortcoming of current
414 inactivated vaccines. Alternatively, the manipulation of RNA structures such as SL9, to
415 provide attenuation in bovine cells but retain efficient growth in vaccine production cell
416 lines (BHK), could be used to enhance biosafety of inactivated vaccine production. The
417 hazards associated with the large-scale production of killed vaccine viruses include both
418 accidental release of virus from high containment production facilities, and the
419 distribution and use of improperly inactivated FMD vaccines (79-81).

420 In summary, we have generated a comprehensive map of RNA secondary
421 structure located within the ORF of the FMDV genome and identified novel stem-loops
422 within the coding region for $3D^{pol}$ that appear critical for FMDV replication. While the
423 function of the other conserved structures remains to be determined they can be

424 targeted to improve understanding of the FMDV biology. In addition, they have the
425 potential to help develop safer FMDV vaccines, an idea which has been proposed for
426 other viruses (6, 56, 82). We also show that usage of the CDLR algorithm can be
427 successfully utilised to permute RNA sequences in search of functional RNA structures,
428 which can be applied beyond viral RNA molecules using a freely available and easy to
429 use package (60).

430 **MATERIALS AND METHODS**

431 **Cell lines.** Madin-Darby bovine kidney (MDBK) and baby hamster kidney (BHK-
432 21) cells were obtained from the American Type Culture Collection (ATCC) and
433 maintained in Dulbecco's Modified Eagle Medium containing either 10% foetal bovine
434 serum (FBS) or 10% horse serum (MDBK cells) at 37 °C and 5% CO_2.

435 **FMDV sequence dataset.** Full genome sequences of 105 viruses were selected
436 from GenBank database based on nucleotide distance of their 1D encoding region,
437 ensuring that they represent sequence variability that is known to be present between
438 all seven FMDV serotypes (Table 5). Since sequences of SAT serotypes are the least
439 represented on public databases, 13 additional full genome sequences of field SAT
440 isolates (SAT 1 = 2, SAT 2 = 4 and SAT 3 = 7) were generated for the purpose of this
441 study (isolates: SAT1/TAN/3/80, SAT1/ZAM/2/88, SAT2/BOT-BUFF/7/72,
442 SAT2/MOZ/1/70, SAT2/ZAM-BUFF/18/74, SAT2/ZIM/8/89, SAT3/BOT/209/67,
443 SAT3/RHO/26/76, SAT3/RHO/3/75, SAT3/SAR/9/79, SAT3/ZAM/P2/96(MUL-4),
444 SAT3/ZIM/P25/91(UR-7), SAT3/ZIM/P26/90(HV-5) using methodology previously
445 described (45).

Prediction of conserved RNA structures within the FMDV genome. The genomic sequences of the 118 FMDV field isolates were aligned using the MAFFT X-INS-i algorithm which, in addition to nucleotide identity, takes into account RNA secondary structure information (83, 84). This approach minimized the potential to overlook conserved RNA structures that might be hidden in a nucleotide alignment containing distantly related FMDV sequences. The multiple sequence alignment (MSA) was analysed using the RNAalifold program implemented in The ViennaRNA Package (61), using the following options: a ribosum scoring matrix, calculating the partition function and base pairing probability matrix in addition to the minimum free energy (MFE) structure, producing structure without lonely pairs and with dangling energies added for the bases adjacent to a helix on both sides. Then, the conserved RNA structures in the full genome were 'tidied up' by removing gaps and long-distance interactions (i.e., interactions which were separated by 400 nucleotides or more). The same was repeated for each FMDV serotype individually (using the dataset described above) and serotype-specific conserved RNA structure prediction was compared to the conserved structure prediction for all 118 FMDV sequences. Only stem-loops which were verified in all seven FMDV serotypes were considered as highly conserved. Finally, the conserved, whole genome FMDV RNA structure was visualised by drawing a dot plot graph using an awk script written *in house* and available upon request. To visualise shorter genomic fragments containing predicted conserved RNA structure(s) (e.g., the 3' terminal part of the $3D^{pol}$ encoding region and individual loops) in more detail, a particular genomic region together with its conserved structure prediction was extracted and visualised using an on-line Forna tool implemented in The ViennaRNA Web Services (85). The extent of nucleotide conservation in sequence forming hairpin

loops of RNA structures (Fig. 5) was visualised using WebLogo 3.7.4 web server (86, 87).

Pairwise distance and MFED for full genome sequences of all seven FMDV serotypes (dataset described above) were prepared using the Sequence Distances and Folding Energy Scan programs implemented in SSE v1.4 package (60), respectively. The MSA for MFED analysis was prepared as described above, while controls for calculation of MFED were generated by the NDR algorithm. For sequence distance analysis the FMDV genomes were separated into three genomic regions: the 5' UTR, the ORF and the 3' UTR which were aligned individually by different MAFFT algorithms. The 5' and 3' UTRs were aligned by MAFFT X-INS-i, while the nucleotide sequence of the ORF was firstly converted into amino acid sequence using TRANSEQ EMBOS program (88), aligned using MAFFT G-INS-i (89) and then such generated amino acid alignment was converted into nucleotide sequence using TRANALIGN EMBOS program (88). All aligned genomic fragments were manually combined into a single MSA containing FMDV whole genomes. For both analyses the mean values for successive 400 base fragments with 20 nucleotide increment across the genome were plotted.

The average MFED values of the regions encoding the nsps of the FMDV isolates (i.e., dataset described above), the ptGFP-replicon and 50 CDLR-permuted ptGFP mutants were calculated as described above.

Since there appears to be a lot of ambiguity around the poly(C) tract, that region and its flanking positions were excluded from all analyses.

***In silico* design of mutants containing modified segments within the non-structural encoding region.** The regions encoding the nsps of the FMDV genome were chosen for mutagenesis by restriction site usage (sequence listed in Fig. 3A-B). To disrupt RNA secondary structures predicted in each restriction fragment of native FMDV genomes, sequences were mutated using the CDLR algorithm implemented in the Scramble Sequences Program of the SSE v1.4 package.

Structure prediction of the 3' terminal part of the $3D^{pol}$ encoding region of the WT replicon which was scrambled by the CDLR algorithm (the $3D_3$ region) was generated as described above but using RNAfold (61), and using parameters corresponding to the ones applied in RNAalifold. The predicted structure was visualised in Forna.

To 'quantify' the difference between structure of the WT and scrambled replicons (Fig. 3A-B, Table 2), the whole genomic sequence of WT and each scrambled replicon was predicted using RNAfold, and fragments of the RNA secondary structure prediction corresponding to the permutated regions encoding the nsps (Fig. 3A-B) were compared using RNAforester and global alignment, with the relative scores as a measure of structure similarity (61, 63, 64).

For each predicted RNA structure located at the 3' terminal part of the FMDV $3D^{pol}$ encoding region (SL7 - SL11 in the $3D_3$ region) nucleotides were changed manually (see results section). Individual putative stem-loops and their mutants were predicted using RNAfold implemented in The ViennaRNA package and mfold RNA structure prediction server (90), and were visualised using Forna RNA secondary structure visualisation tool.

Comparison of putative RNA structures located within 3' terminal 3D^{pol} encoding region of FMDV and PV. Computational prediction of two conserved PV RNA structures located in the 3' terminal 3D^{pol} encoding region (termed loop α and β as in Song *et. al.* 2012) and described previously (37, 38) was repeated as described above. This was done as there was some discrepancy between the two publications about the exact structure of the two PV stem-loops. PV sequences representing variability of the PV 3D encoding region (GenBank accession numbers: NC_002058.3, DQ890388.1, FJ769378.1, EU794963.1, AY560657.1, HF913427.1, EU794957.1, EU794956.1, AF538842.1, EU684057.1, AF405667.1, AF405666.1, KJ170457.1, KJ170438.1, KU866422.1, AM884184.1, AJ132961.1, MG212491.1, MG212488.1, MG212485.1, MG212463.1, MG212456.1, MG212441.1, MG212440.1, KY941933.1, KY941932.1, KR259355.1, KC784372.1, KC880377.1, JX275352.1, JX274995.1, KX162704.1) were used. The RNA loop α and β were isolated and their structure aligned to the 3' terminal part of the 3D^{pol} encoding region containing FMDV stem-loops SL7 - SL11 ($3D_3$ region) using the RNAforester software and 'small-in-large similarity' calculation to determine whether any of the previously described PV stem-loops were similar to any of the FMDV RNA structures identified in this study. For more detailed analysis, each isolated FMDV putative RNA stem-loop (SL7 - SL11) was directly compared to PV loop α or β using RNAforester as described above.

Clone construction. Sequences with mutations generated by the CDLR algorithm and nucleotide fragments containing mutated loops SL7 – SL11 were synthesised by custom DNA synthesis (GeneArt, Life Technologies) and provided within standard cloning vectors. These sequences were firstly sub-cloned into the pSP72

vector (Promega) to provide the unique restriction enzyme sites for subsequent cloning into the WT ptGFP replicon (Fig. 3A; (65)).

***In vitro* transcription.** Replicon constructs (5 µg) were linearised with AscI (New England Biolabs) for 1 h at 37 °C and purified using the E.Z.N.A. ™ Gel Extraction Kit (Omega Bio-Tek). Linear replicon DNA (500 ng) was added to transcription reactions at a final volume of 100 µl containing the following: Transcription Optimised Buffer (Promega), 10 mM DTT (Promega), 100 U RNasin Ribonuclease Inhibitor (Promega), 40 U T7 RNA polymerase (Promega), 20 mM rNTP's (Promega) and nuclease-free water. Reactions were incubated at 37 °C for 2 h and the resulting transcript integrity assessed by agarose gel electrophoresis. RNA yield was quantified using the Quantus ™ Fluorometer (Promega), according to the manufacturer's instructions.

Cell transfection. Approximately 20 h prior to transfection cells were seeded into 24 or 12 well plates at the appropriate cell seeding density to achieve ~ 80% confluency. The following day, media was removed and replaced with FluoroBrite™ DMEM (Gibco) supplemented with 2% FBS and 4 mM glutamine. Replicon transcript RNA (0.5-1 µg) was transfected into triplicate or quadruplicate cell monolayers using Lipofectamine 2000 transfection reagent as per the manufacturer's recommendation (Thermo Fisher Scientific).

Live cell imaging. Live cell image analysis was performed using the IncuCyte ZOOM kinetic imaging system (Essen BioScience) as described previously (62). Images were captured hourly for a period of 24 h with green fluorescent protein intensity measured using the integrated IncuCyte ZOOM image processing software. Data are

558 shown as the average cell (green object) GFP intensity per well at 8 h post-transfection
559 (where expression is at the maximum level).

560 **Statistical analysis.** Replicon mutants were compared to WT ptGFP using one-
561 way analysis of variance (ANOVA). Differences between groups were considered to be
562 significant at a *P* value of <0.05 (*), <0.01 (**) or <0.001 (***). Error bars represent
563 standard error of the mean (S.E.M.) of multiple independent experiments. Statistical
564 analyses were performed with GraphPad Prism 8.00 (GraphPad Software, San Diego,
565 California USA, www.graphpad.com).

566 **Data availability.** Full genome FMDV sequences generated as a part of this
567 study were submitted to GenBank and are available as following accession numbers:
568 MW355668 - MW355680.

569 **ACKNOWLEDGMENTS**

570 We thank colleagues in the WRLFMD (Pirbright, UK) for providing the FMDV
571 isolates used in this study. The Pirbright Institute receives grant-aided support from the
572 Biotechnology and Biological Sciences Research Council (BBSRC) of the United
573 Kingdom (projects BB/E/I/00007035, BB/E/I/00007036 and BBS/E/I/00007037)
574 providing funds to cover the open access charges for this paper. This work was
575 supported by funding from UK Department for Environment, Food and Rural Affairs
576 (Defra research project SE2943) and BBSRC research grant BB/K003801/1.

577 **Author Contributions.** Lidia Lasecka-Dykes, Paolo Ribeca and Peter Simmonds
578 performed bioinformatic analyses; Fiona Tulloch, Garry A. Luke, Lidia Lasecka-Dykes
579 and Sarah Gold carried out experimental work and analysed data; Nick J. Knowles,

Jemma Wadsworth and Mehreen Azhar selected and isolated viruses; Lidia Lasecka-Dykes and Caroline F. Wright sequenced FMDV isolates and analysed sequencing data; Fiona Tulloch, Lidia Lasecka-Dykes, Terry Jackson, Tobias J. Tuthill, Martin D. Ryan, Peter Simmonds and Donald P. King conceived and designed the experiments; Martin D. Ryan, Terry Jackson, Tobias J. Tuthill and Donald P. King directed the study; Martin D. Ryan, Terry Jackson, Tobias J. Tuthill and Donald P. King acquisitioned the funding; Lidia Lasecka-Dykes, Fiona Tulloch and Peter Simmonds wrote the initial draft of the manuscript; all authors reviewed and edited the manuscript.

Conflicts of Interest. The authors declare no conflict of interest. The funders had no role in the design of the study; in the collection, analyses, or interpretation of data; in the writing of the manuscript, and in the decision to publish the results.

REFERENCES

1. Wang J, Bakkers JM, Galama JM, Bruins Slot HJ, Pilipenko EV, Agol VI, Melchers WJ. 1999. Structural requirements of the higher order RNA kissing element in the enteroviral 3'UTR. Nucleic Acids Res 27:485-90.
2. Watts JM, Dang KK, Gorelick RJ, Leonard CW, Bess JW, Jr., Swanstrom R, Burch CL, Weeks KM. 2009. Architecture and secondary structure of an entire HIV-1 RNA genome. Nature 460:711-6.
3. Wu B, Grigull J, Ore MO, Morin S, White KA. 2013. Global organization of a positive-strand RNA virus genome. PLoS Pathog 9:e1003363.
4. Dethoff EA, Boerneke MA, Gokhale NS, Muhire BM, Martin DP, Sacco MT, McFadden MJ, Weinstein JB, Messer WB, Horner SM, Weeks KM. 2018.

602 Pervasive tertiary structure in the dengue virus RNA genome. Proceedings of the
603 National Academy of Sciences of the United States of America 115:11513-
604 11518.
605 5. Thurner C, Witwer C, Hofacker IL, Stadler PF. 2004. Conserved RNA secondary
606 structures in Flaviviridae genomes. J Gen Virol 85:1113-1124.
607 6. Firth AE. 2014. Mapping overlapping functional elements embedded within the
608 protein-coding regions of RNA viruses. Nucleic Acids Res 42:12425-39.
609 7. Akiyama BM, Laurence HM, Massey AR, Costantino DA, Xie XP, Yang YJ, Shi
610 PY, Nix JC, Beckham JD, Kieft JS. 2016. Zika virus produces noncoding RNAs
611 using a multi-pseudoknot structure that confounds a cellular exonuclease.
612 Science 354:1148-1152.
613 8. Tuplin A, Evans DJ, Simmonds P. 2004. Detailed mapping of RNA secondary
614 structures in core and NS5B-encoding region sequences of hepatitis C virus by
615 RNase cleavage and novel bioinformatic prediction methods. J Gen Virol
616 85:3037-3047.
617 9. Ferhadian D, Contrant M, Printz-Schweigert A, Smyth RP, Paillart JC, Marquet R.
618 2018. Structural and Functional Motifs in Influenza Virus RNAs. Front Microbiol
619 9:559.
620 10. Michalak P, Soszynska-Jozwiak M, Biala E, Moss WN, Kesy J, Szutkowska B,
621 Lenartowicz E, Kierzek R, Kierzek E. 2019. Secondary structure of the segment 5
622 genomic RNA of influenza A virus and its application for designing antisense
623 oligonucleotides. Sci Rep 9:3801.
624 11. Simmonds P, Karakasiliotis I, Bailey D, Chaudhry Y, Evans DJ, Goodfellow IG.
625 2008. Bioinformatic and functional analysis of RNA secondary structure elements

among different genera of human and animal caliciviruses. Nucleic Acids Res 36:2530-46.

12. Witwer C, Rauscher S, Hofacker IL, Stadler PF. 2001. Conserved RNA secondary structures in Picornaviridae genomes. Nucleic Acids Res 29:5079-89.

13. Tuplin A. 2015. Diverse roles and interactions of RNA structures during the replication of positive-stranded RNA viruses of humans and animals. J Gen Virol 96:1497-503.

14. Alexandersen S, Zhang Z, Donaldson AI, Garland AJ. 2003. The pathogenesis and diagnosis of foot-and-mouth disease. J Comp Pathol 129:1-36.

15. Kitching RP. 1999. Foot-and-mouth disease: current world situation. Vaccine 17:1772-4.

16. King DP, Henstock M. 2016. OIE/FAO Foot-and-Mouth Disease Reference Laboratory Network Annual Report 2016.

17. Gloster J, Sellers RF, Donaldson AI. 1982. Long-Distance Transport of Foot-and-Mouth-Disease Virus over the Sea. Veterinary Record 110:47-52.

18. Scudamore JM, Harris DM. 2002. Control of foot and mouth disease: lessons from the experience of the outbreak in Great Britain in 2001. Revue Scientifique Et Technique De L Office International Des Epizooties 21:699-710.

19. Knowles NJ, Samuel AR. 2003. Molecular epidemiology of foot-and-mouth disease virus. Virus Res 91:65-80.

20. Rweyemamu M, Roeder P, Mackay D, Sumption K, Brownlie J, Leforban Y, Valarcher JF, Knowles NJ, Saraiva V. 2008. Epidemiological patterns of foot-and-mouth disease worldwide. Transbound Emerg Dis 55:57-72.

649 21. Weaver GV, Domenech J, Thiermann AR, Karesh WB. 2013. Foot and mouth
650 disease: a look from the wild side. J Wildl Dis 49:759-85.
651 22. Di Nardo A, Knowles NJ, Paton DJ. 2011. Combining livestock trade patterns
652 with phylogenetics to help understand the spread of foot and mouth disease in
653 sub-Saharan Africa, the Middle East and Southeast Asia. Rev Sci Tech 30:63-85.
654 23. Samuel AR, Knowles NJ. 2001. Foot-and-mouth disease type O viruses exhibit
655 genetically and geographically distinct evolutionary lineages (topotypes). J Gen
656 Virol 82:609-21.
657 24. Kitching P, Hammond J, Jeggo M, Charleston B, Paton D, Rodriguez L, Heckert
658 R. 2007. Global FMD control - Is it an option? Vaccine 25:5660-5664.
659 25. Mason PW, Grubman MJ, Baxt B. 2003. Molecular basis of pathogenesis of
660 FMDV. Virus Res 91:9-32.
661 26. Ryan MD, Belsham GJ, King AM. 1989. Specificity of enzyme-substrate
662 interactions in foot-and-mouth disease virus polyprotein processing. Virology
663 173:35-45.
664 27. Strebel K, Beck E. 1986. A second protease of foot-and-mouth disease virus. J
665 Virol 58:893-9.
666 28. Vakharia VN, Devaney MA, Moore DM, Dunn JJ, Grubman MJ. 1987. Proteolytic
667 processing of foot-and-mouth disease virus polyproteins expressed in a cell-free
668 system from clone-derived transcripts. J Virol 61:3199-207.
669 29. Klump W, Marquardt O, Hofschneider PH. 1984. Biologically-Active Protease of
670 Foot and Mouth-Disease Virus Is Expressed from Cloned Viral Cdna in
671 Escherichia-Coli. Proceedings of the National Academy of Sciences of the United
672 States of America-Biological Sciences 81:3351-3355.

673 30. Belsham GJ. 2005. Translation and replication of FMDV RNA. Curr Top Microbiol
674 Immunol 288:43-70.
675 31. Donnelly MLL, Luke G, Mehrotra A, Li XJ, Hughes LE, Gani D, Ryan MD. 2001.
676 Analysis of the aphthovirus 2A/2B polyprotein 'cleavage' mechanism indicates
677 not a proteolytic reaction, but a novel translational effect: a putative ribosomal
678 'skip'. Journal of General Virology 82:1013-1025.
679 32. Doronina VA, Wu C, de Felipe P, Sachs MS, Ryan MD, Brown JD. 2008. Site-
680 specific release of nascent chains from ribosomes at a sense codon. Mol Cell
681 Biol 28:4227-39.
682 33. Ryan MD, Donnelly M, Lewis A, Mehrotra AP, Wilkie J, Gani D. 1999. A model
683 for nonstoichiometric, cotranslational protein scission in eukaryotic ribosomes.
684 Bioorganic Chemistry 27:55-79.
685 34. Ryan MD, King AM, Thomas GP. 1991. Cleavage of foot-and-mouth disease
686 virus polyprotein is mediated by residues located within a 19 amino acid
687 sequence. J Gen Virol 72 (Pt 11):2727-32.
688 35. Jackson RJ, Howell MT, Kaminski A. 1990. The novel mechanism of initiation of
689 picornavirus RNA translation. Trends Biochem Sci 15:477-83.
690 36. McKnight KL, Lemon SM. 1998. The rhinovirus type 14 genome contains an
691 internally located RNA structure that is required for viral replication. RNA 4:1569-
692 84.
693 37. Burrill CP, Westesson O, Schulte MB, Strings VR, Segal M, Andino R. 2013.
694 Global RNA structure analysis of poliovirus identifies a conserved RNA structure
695 involved in viral replication and infectivity. J Virol 87:11670-83.

696 38. Song Y, Liu Y, Ward CB, Mueller S, Futcher B, Skiena S, Paul AV, Wimmer E.
697 2012. Identification of two functionally redundant RNA elements in the coding
698 sequence of poliovirus using computer-generated design. Proc Natl Acad Sci U S
699 A 109:14301-7.
700 39. Rieder E, Paul AV, Kim DW, van Boom JH, Wimmer E. 2000. Genetic and
701 biochemical studies of poliovirus cis-acting replication element cre in relation to
702 VPg uridylylation. J Virol 74:10371-80.
703 40. Kloc A, Rai DK, Rieder E. 2018. The Roles of Picornavirus Untranslated Regions
704 in Infection and Innate Immunity. Front Microbiol 9:485.
705 41. Clarke BE, Brown AL, Currey KM, Newton SE, Rowlands DJ, Carroll AR. 1987.
706 Potential Secondary and Tertiary Structure in the Genomic Rna of Foot-and-
707 Mouth-Disease Virus. Nucleic Acids Research 15:7067-7079.
708 42. Kloc A, Diaz-San Segundo F, Schafer EA, Rai DK, Kenney M, de Los Santos T,
709 Rieder E. 2017. Foot-and-mouth disease virus 5'-terminal S fragment is required
710 for replication and modulation of the innate immune response in host cells.
711 Virology 512:132-143.
712 43. Serrano P, Pulido MR, Saiz M, Martinez-Salas E. 2006. The 3' end of the foot-
713 and-mouth disease virus genome establishes two distinct long-range RNA-RNA
714 interactions with the 5' end region. J Gen Virol 87:3013-22.
715 44. Newton SE, Carroll AR, Campbell RO, Clarke BE, Rowlands DJ. 1985. The
716 sequence of foot-and-mouth disease virus RNA to the 5' side of the poly(C) tract.
717 Gene 40:331-6.
718 45. Lasecka-Dykes L, Wright CF, Di Nardo A, Logan G, Mioulet V, Jackson T, Tuthill
719 TJ, Knowles NJ, King DP. 2018. Full Genome Sequencing Reveals New

720 Southern African Territories Genotypes Bringing Us Closer to Understanding
721 True Variability of Foot-and-Mouth Disease Virus in Africa. Viruses-Basel 10.
722 46. Zhu Z, Yang F, Cao W, Liu H, Zhang K, Tian H, Dang W, He J, Guo J, Liu X,
723 Zheng H. 2019. The Pseudoknot Region of the 5' Untranslated Region Is a
724 Determinant of Viral Tropism and Virulence of Foot-and-Mouth Disease Virus. J
725 Virol 93.
726 47. Lopez de Quinto S, Martinez-Salas E. 1997. Conserved structural motifs located
727 in distal loops of aphthovirus internal ribosome entry site domain 3 are required
728 for internal initiation of translation. J Virol 71:4171-5.
729 48. Belsham GJ, Brangwyn JK. 1990. A region of the 5' noncoding region of foot-
730 and-mouth disease virus RNA directs efficient internal initiation of protein
731 synthesis within cells: involvement with the role of L protease in translational
732 control. J Virol 64:5389-95.
733 49. Kuhn R, Luz N, Beck E. 1990. Functional analysis of the internal translation
734 initiation site of foot-and-mouth disease virus. J Virol 64:4625-31.
735 50. Serrano P, Ramajo J, Martinez-Salas E. 2009. Rescue of internal initiation of
736 translation by RNA complementation provides evidence for a distribution of
737 functions between individual IRES domains. Virology 388:221-9.
738 51. Mason PW, Bezborodova SV, Henry TM. 2002. Identification and
739 characterization of a cis-acting replication element (cre) adjacent to the internal
740 ribosome entry site of foot-and-mouth disease virus. J Virol 76:9686-94.
741 52. Nayak A, Goodfellow IG, Belsham GJ. 2005. Factors required for the
742 Uridylylation of the foot-and-mouth disease virus 3B1, 3B2, and 3B3 peptides by
743 the RNA-dependent RNA polymerase (3Dpol) in vitro. J Virol 79:7698-706.

744 53. Saiz M, Gomez S, Martinez-Salas E, Sobrino F. 2001. Deletion or substitution of
745 the aphthovirus 3' NCR abrogates infectivity and virus replication. J Gen Virol
746 82:93-101.
747 54. Pulido MR, Sobrino F, Borrego B, Saiz M. 2009. Attenuated Foot-and-Mouth
748 Disease Virus RNA Carrying a Deletion in the 3 ' Noncoding Region Can Elicit
749 Immunity in Swine. Journal of Virology 83:3475-3485.
750 55. Logan G, Newman J, Wright CF, Lasecka-Dykes L, Haydon DT, Cottam EM,
751 Tuthill TJ. 2018. Deep Sequencing of Foot-and-Mouth Disease Virus Reveals
752 RNA Sequences Involved in Genome Packaging. Journal of Virology 92.
753 56. Simmonds P, Tuplin A, Evans DJ. 2004. Detection of genome-scale ordered
754 RNA structure (GORS) in genomes of positive-stranded RNA viruses:
755 Implications for virus evolution and host persistence. RNA 10:1337-51.
756 57. Rivas E, Eddy SR. 2000. Secondary structure alone is generally not statistically
757 significant for the detection of noncoding RNAs. Bioinformatics 16:583-605.
758 58. Workman C, Krogh A. 1999. No evidence that mRNAs have lower folding free
759 energies than random sequences with the same dinucleotide distribution. Nucleic
760 Acids Res 27:4816-22.
761 59. Davis M, Sagan SM, Pezacki JP, Evans DJ, Simmonds P. 2008. Bioinformatic
762 and physical characterizations of genome-scale ordered RNA structure in
763 mammalian RNA viruses. J Virol 82:11824-36.
764 60. Simmonds P. 2012. SSE: a nucleotide and amino acid sequence analysis
765 platform. BMC Res Notes 5:50.
766 61. Lorenz R, Bernhart SH, Honer Zu Siederdissen C, Tafer H, Flamm C, Stadler PF,
767 Hofacker IL. 2011. ViennaRNA Package 2.0. Algorithms Mol Biol 6:26.

768 62. Tulloch F, Pathania U, Luke GA, Nicholson J, Stonehouse NJ, Rowlands DJ,
769 Jackson T, Tuthill T, Haas J, Lamond AI, Ryan MD. 2014. FMDV replicons
770 encoding green fluorescent protein are replication competent. J Virol Methods
771 209:35-40.
772 63. Hoechsmann M, Toeller T, Giegerich R, Kurtz S. Local Similarity of RNA
773 Secondary Structures, p 159-168. *In* (ed),
774 64. Jiang T, Wang LS, Zhang KZ. 1995. Alignment of Trees - an Alternative to Tree
775 Edit. Theoretical Computer Science 143:137-148.
776 65. Herod MR, Loundras EA, Ward JC, Tulloch F, Rowlands DJ, Stonehouse NJ.
777 2015. Employing transposon mutagenesis to investigate foot-and-mouth disease
778 virus replication. J Gen Virol 96:3507-3518.
779 66. Simmonds P, Cuypers L, Irving WL, McLauchlan J, Cooke GS, Barnes E,
780 Consortium S-H, Ansari MA. 2020. Impact of virus subtype and host IFNL4
781 genotype on large-scale RNA structure formation in the genome of hepatitis C
782 virus. RNA 26:1541-1556.
783 67. Pirakitikulr N, Kohlway A, Lindenbach BD, Pyle AM. 2016. The Coding Region of
784 the HCV Genome Contains a Network of Regulatory RNA Structures. Mol Cell
785 62:111-20.
786 68. Mauger DM, Golden M, Yamane D, Williford S, Lemon SM, Martin DP, Weeks
787 KM. 2015. Functionally conserved architecture of hepatitis C virus RNA
788 genomes. Proc Natl Acad Sci U S A 112:3692-7.
789 69. Luna VER, Luk ADH, Tyring SK, Hellman JM, Lefkowitz SS. 1984. Properties of
790 Bovine Interferons. Experientia 40:1410-1412.

791 70. Conzelmann KK. 2004. Reverse genetics of Mononegavirales. Biology of
792 Negative Strand Rna Viruses: The Power of Reverse Genetics 283:1-41.
793 71. Schlender J, Bossert B, Buchholz U, Conzelmann KK. 2000. Bovine respiratory
794 syncytial virus nonstructural proteins NS1 and NS2 cooperatively antagonize
795 alpha/beta interferon-induced antiviral response. J Virol 74:8234-42.
796 72. Witteveldt J, Blundell R, Maarleveld JJ, McFadden N, Evans DJ, Simmonds P.
797 2014. The influence of viral RNA secondary structure on interactions with innate
798 host cell defences. Nucleic Acids Research 42:3314-3329.
799 73. Smyth RP, Negroni M, Lever AM, Mak J, Kenyon JC. 2018. RNA Structure-A
800 Neglected Puppet Master for the Evolution of Virus and Host Immunity. Front
801 Immunol 9:2097.
802 74. Zhang ZD, Alexandersen S. 2004. Quantitative analysis of foot-and-mouth
803 disease virus RNA loads in bovine tissues: implications for the site of viral
804 persistence. Journal of General Virology 85:2567-2575.
805 75. Condy JB, Hedger RS, Hamblin C, Barnett IT. 1985. The duration of the foot-and-
806 mouth disease virus carrier state in African buffalo (i) in the individual animal and
807 (ii) in a free-living herd. Comp Immunol Microbiol Infect Dis 8:259-65.
808 76. Vosloo W, Dwarka RM, Bastos ADS, Esterhuysen JJ, Sahle M, Sangare O.
809 2004. Molecular epidemiological studies of foot-and-mouth disease virus in sub-
810 Saharan Africa indicate the presence of large numbers of topotypes: implications
811 for local and international control. .
812 77. Vosloo W, de Klerk LM, Boshoff CI, Botha B, Dwarka RM, Keet D, Haydon DT.
813 2007. Characterisation of a SAT-1 outbreak of foot-and-mouth disease in captive

814 African buffalo (Syncerus caffer): clinical symptoms, genetic characterisation and
815 phylogenetic comparison of outbreak isolates. Vet Microbiol 120:226-40.
816 78. Thomson GR, Vosloo W, Esterhuysen JJ, Bengis RG. 1992. Maintenance of foot
817 and mouth disease viruses in buffalo (Syncerus caffer Sparrman, 1779) in
818 southern Africa. Rev Sci Tech 11:1097-107.
819 79. Spratt BG. 2007. Independent Review of the safety of UK facilities handling foot-
820 and-mouth disease virus.
821 80. Callaghan B. 2007. A review of the regulatory framework for handling animal
822 pathogens.
823 81. Sangula AK, Siegismund HR, Belsham GJ, Balinda SN, Masembe C, Muwanika
824 VB. 2011. Low diversity of foot-and-mouth disease serotype C virus in Kenya:
825 evidence for probable vaccine strain re-introductions in the field. Epidemiol Infect
826 139:189-96.
827 82. Runckel C, Westesson O, Andino R, DeRisi JL. 2013. Identification and
828 manipulation of the molecular determinants influencing poliovirus recombination.
829 PLoS Pathog 9:e1003164.
830 83. Katoh K, Toh H. 2008. Improved accuracy of multiple ncRNA alignment by
831 incorporating structural information into a MAFFT-based framework. BMC
832 Bioinformatics 9:212.
833 84. Katoh K, Asimenos G, Toh H. 2009. Multiple alignment of DNA sequences with
834 MAFFT. Methods Mol Biol 537:39-64.
835 85. Kerpedjiev P, Hammer S, Hofacker IL. 2015. Forna (force-directed RNA): Simple
836 and effective online RNA secondary structure diagrams. Bioinformatics 31:3377-
837 9.

838 86. Schneider TD, Stephens RM. 1990. Sequence logos: a new way to display
839 consensus sequences. Nucleic Acids Res 18:6097-100.
840 87. Crooks GE, Hon G, Chandonia JM, Brenner SE. 2004. WebLogo: a sequence
841 logo generator. Genome Res 14:1188-90.
842 88. Madeira F, Park YM, Lee J, Buso N, Gur T, Madhusoodanan N, Basutkar P,
843 Tivey ARN, Potter SC, Finn RD, Lopez R. 2019. The EMBL-EBI search and
844 sequence analysis tools APIs in 2019. Nucleic Acids Res 47:W636-W641.
845 89. Katoh K, Kuma K, Toh H, Miyata T. 2005. MAFFT version 5: improvement in
846 accuracy of multiple sequence alignment. Nucleic Acids Res 33:511-8.
847 90. Zuker M. 2003. Mfold web server for nucleic acid folding and hybridization
848 prediction. Nucleic Acids Res 31:3406-15.

849

850

851 **Table 1**

852 Number of conserved stem-loops within each FMDV genomic region

Genomic region	Number of predicted stem-loops[a]
S-fragment	1
The rest of 5' UTR[b]	11[*]
L^{pro}	4
1A (VP4)	0
1B (VP2)	1
1C (VP3)	1
1 (VP1)	2
2A	1[**]
2B	7
2C	10
3A	3
$3B_1$	1
$3B_2$	2
$3B_3$	1[***]
3C	3
3D	17
3' UTR	2

853 [a]Each hairpin loop was counted individually;

854 [b]Excludes poly(C) tract and pseudoknot regions;

855 [*]*cre* (a single hairpin loop), IRES domain 2 (a single hairpin loop), IRES domain 3 (five

856 hairpin loops), IRES domain 4 (two hairpin loops), IRES domain 5 (a single hairpin

857 loop), plus a single hairpin loop downstream of IRES;

858 [**]Four nucleotides of the 5' end of the stem belong to the 1D encoding region;

859 [***]17 nucleotides of the 5' end of the stem belong to the $3B_3$ encoding region.

Table 2

Similarity comparison of RNA structures within corresponding WT and CDLR replicon genomic fragments, calculated using RNAforester program

	Replicon fragments[a]												
	Δ1D-2B	**2B-2C**	**2C**	**2C-3A**	**3A-3B**	**3B-3C**	**3C-3D$_1$**	**3D$_2$**	**3D$_3$**	**S-fragment**	***cre****	**IRES***	**SL1 and SL2***
WT vs CDLR relative similarity score[b]	-1.33	-0.71	0.24	-0.87	-0.80	-1.69	-1.06	-0.72	-1.66	1	1	1	0.64

[a]nsps encoding regions fragments as presented in Fig. 3A-B

[b]value =1 is for two identical structures: the greater the distance from 1, the less structure similarity between two corresponding fragments. For simplicity, the output of RNAforester was rounded up to two decimal places.

*comparison of RNA structures within the 5' and 3' UTR of the WT and CDLR replicon acts as control (note that while UTR regions were not permutated in this study, there was possibility that permutation of the regions encoding the nsps might affect the pairings within UTRs).

871 **Table 3**

872 Summary of replication profiles of FMDV replicons after mutagenesis of conserved stem-loops localised within the $3D_3$

873 genomic region

	Replicon[a]									
Cell Line	**SL7^{mut}**	**SL8^{mut}**	**SL9^{mut}**	**SL10^{mut}**	**SL11^{mut}**	**SL9,10^{mut}**	**SL9,11^{mut}**	**SL9-11^{mut}**	**SL7-11^{mut}**	**GNN[b]**
BHK-21	WT	WT	94%	52%	WT	27%	60%	28%	23%	11%
MDBK	WT	WT	49%	24%	85%	20%	36%	20%	20%	18%

874

875 [a]See Figure 7 and 8 for study design and data;

876 [b]GNN – replicon with an inactive polymerase, any GFP signal is due to translation;

877 WT – wild type replicon-like replication profile;

878 % - percentage of the WT ptGFP signal, where significant effect on replicon replication was observed.

879

880 **Table 4**

881 Similarity[a] comparison of RNA structures within the $3D^{pol}$ encoding region of FMDV and PV, calculated using RNAforester
882 program

PV \ FMDV	SL7	SL8	SL9	SL10	SL11	*cre**
α	-1.46	-1.83	-2.30	-2.10	-1.85	nd
β	-1.18	-2.07	-2.52	-2.27	-2.07	nd
cre*	nd	nd	nd	nd	nd	0.30

883

884 [a]Relative similarity scores equal to 1 are for two identical structures: the greater the distance from 1, the less structure
885 similarity between two compared features. For simplicity, the output of RNAforester was rounded up to two decimal
886 places.

887 *comparison of *cre* of PV to *cre* of FMDV acts as a control of the structure prediction and RNAforester analysis.

888 **Table 5**

889 FMDV sequences selected from GenBank

Serotype:	Number of isolates:	GenBank accession numbers:
A	19	AY593788, MH053305, JF749843, HM854024, HQ832580, MH053306, KM268896, AY593802, KJ608371, MH053307, AY593751, AY593754, AY593761, AY593764, AY593766, AY593767, HM854022, AY593791, AY593794
Asia 1	12	AY593795, AY687334, DQ533483, DQ989306, DQ989315, DQ989319, EF149010, EF614458, HQ632774, JF739177, KM268898, MF782478
C	6	MH053308, KM268897, MH053309, AJ133357, MH053310, AJ007347
O	21	AY593819, MH053313, MH053311, MH053312, KF112885, KJ206909, HQ632769, HQ632771, KU291242, KR401154, GU384683, KF694737, AJ539140, MH053315, JX040491, MH053317, MH053318, MH053316, KJ560291, DQ404170, KU821591
SAT 1	19	AY593838, AY593845, MH053319, AY593844, JF749860, MH053321, AY593846, AY593839, AY593842, AY593841, AY593840, MH053322, AY593843, KM268899, MH053323, MH053324, MH053325, MH053326, MH053327
SAT2	15	MH053330, MH053332, MH053328, MH053329, JX014255, MH053333, AY593849, JX014256, AY593847, MH053335, KM268900, JF749862, MH053336, MH053337, KU821592
SAT3	13	AY593853, AY593851, MH053339, MH053340, MH053344, MH053343, AY593850, KJ820999, MH053341, MH053351, KX375417, KM268901, MH053350

890

Figure 1

Extent of the conserved RNA secondary structures within FMDV genome

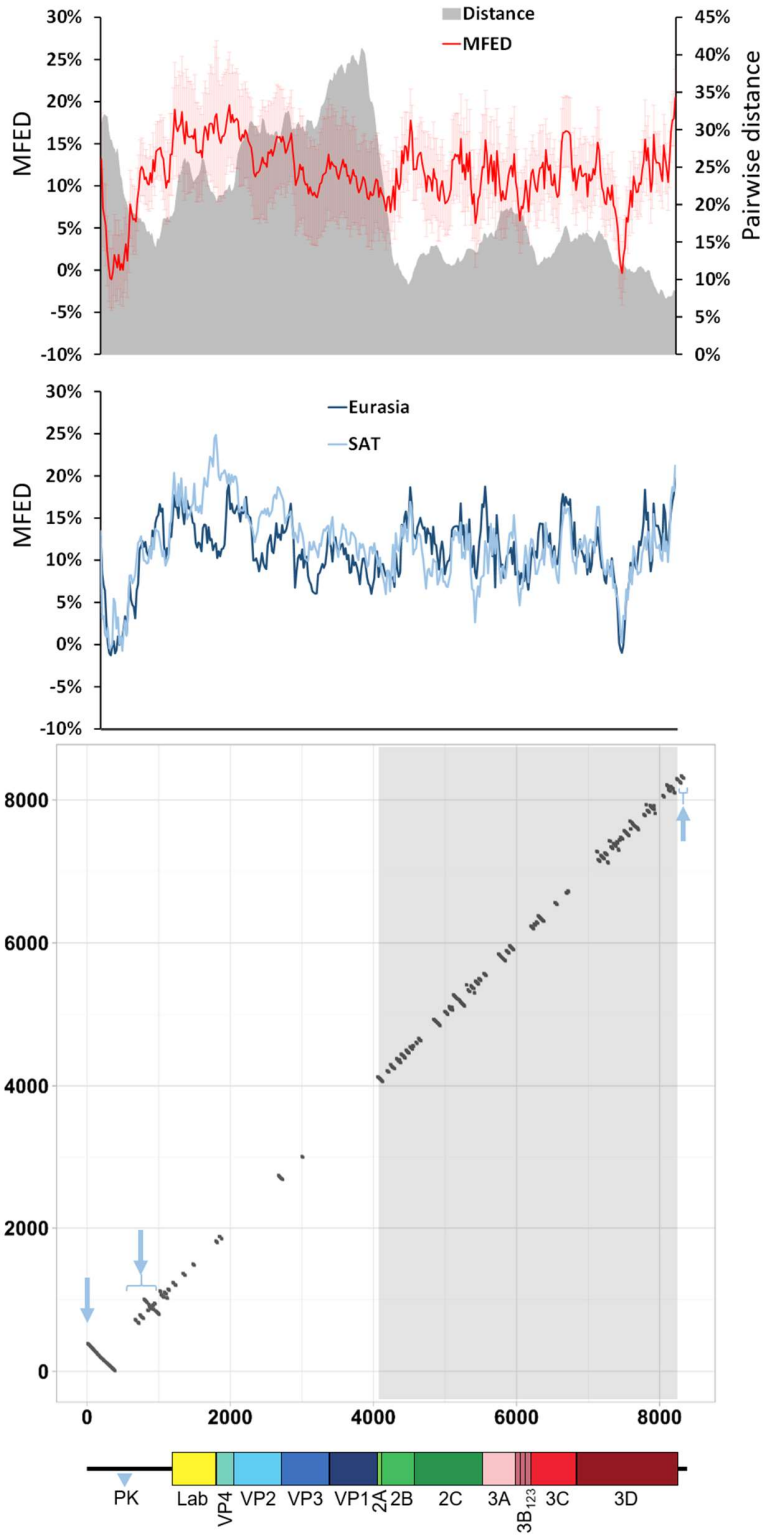

Upper panel shows a scan of pairwise distance and mean folding energies difference (MFED) prepared using SSE v1.4 software and 118 FMDV sequences representing all seven serotypes. The mean values for successive 400 nt fragments across the genome are plotted (where each 400 nts segments overlapped its neighbours by 380 nts). The light red shading represents error bars showing standard deviation from the mean for each datapoint. The middle panel shows MFED values for the same FMDV genomic sequences but grouped into Eurasian (A, Asia 1, C and O serotypes) or SAT (SAT 1 - 3 serotypes) clusters. The lower panel shows a dot plot graphical representation of RNA structures that were conserved across all seven FMDV serotypes. The x-axis and y-axis represent FMDV genome positions, with each dot representing a single pairing between two nucleotides, one with its position marked on the x-axis and the other one with its position marked on the y-axis. The three pale blue arrows indicate location of the S-fragment, *cre*+IRES and SL1+SL2 structures on the dot plot graph, respectively (for a detailed visualisation of these structures see Fig. S1). The blue tringle marked PK indicates the genomic region containing pseudoknot structures which was excluded from these analyses. The area corresponding to the regions encoding the non-structural proteins (i.e., P2 and P3) is highlighted in grey and for clarity, a schematic representation of the FMDV genome is drawn to scale.

933 **Figure 2**

934 Comparison of average MFED values for wild type (WT) and CDLR-scrambled

935 sequences

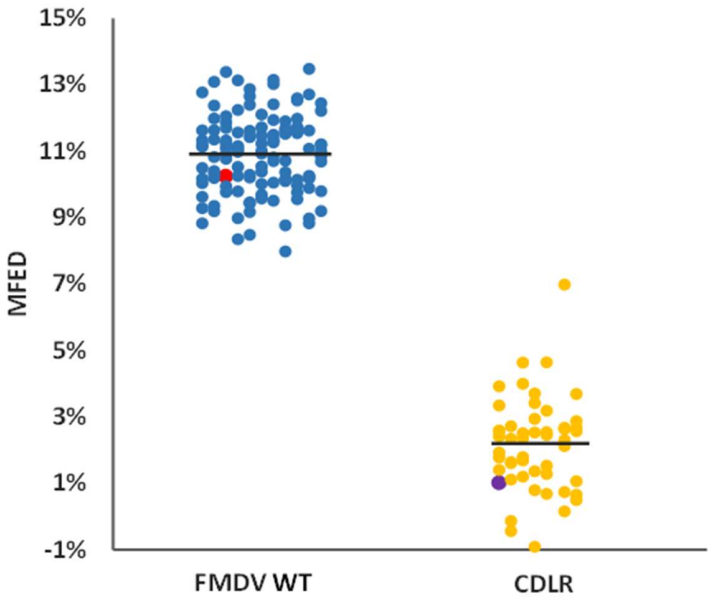

936

937 Mean folding energy difference (MFED) for the regions encoding non-structural proteins
938 (nsps) of 118 FMDV field isolates representing all seven serotypes (blue dots), WT
939 ptGFP-replicon used in this study (red dot) and CDLR scrambled sequences (yellow
940 dots). Among the latter is the CDLR scrambled sequence used in this study to generate
941 replicon mutants (purple dot). To obtain CDLR-scrabbled sequences the sequence of
942 the regions encoding the nsps of the WT replicon was permuted 50 times by codon-
943 shuffling to minimise RNA secondary structure, while preserving protein coding, native
944 dinucleotide frequencies, and codon usage.

945

946 **Figure 3**

947 Replication of CDLR replicons within BHK-21 and MDBK cells

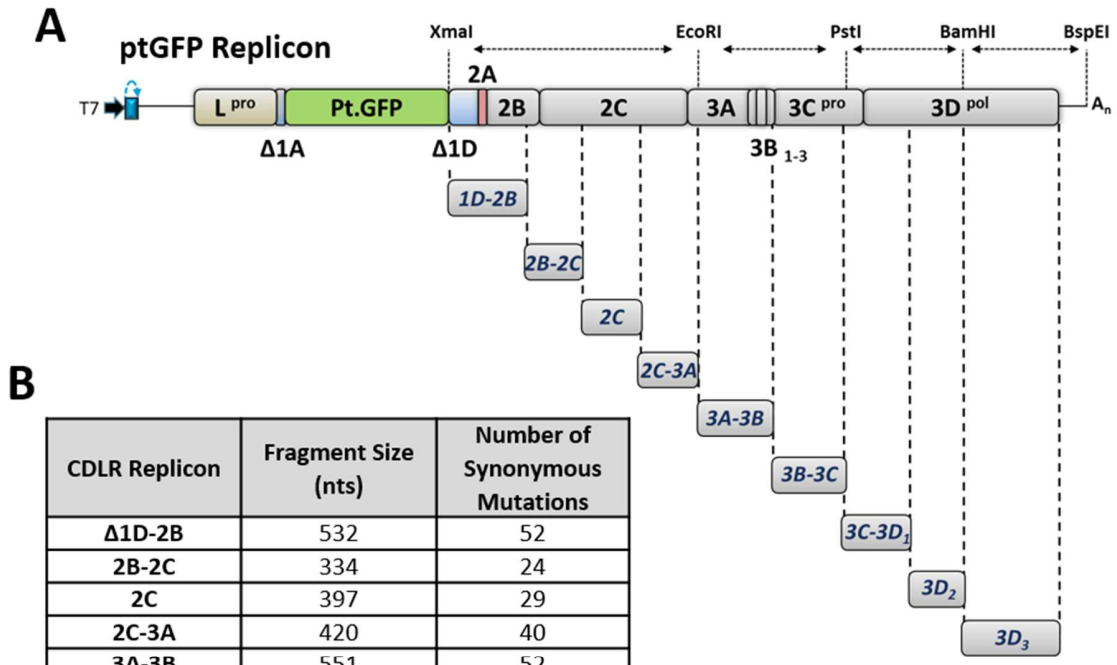

B

CDLR Replicon	Fragment Size (nts)	Number of Synonymous Mutations
Δ1D-2B	532	52
2B-2C	334	24
2C	397	29
2C-3A	420	40
3A-3B	551	52
3B-3C	608	62
3C-3D$_1$	429	36
3D$_2$	596	50
3D$_3$	687	65

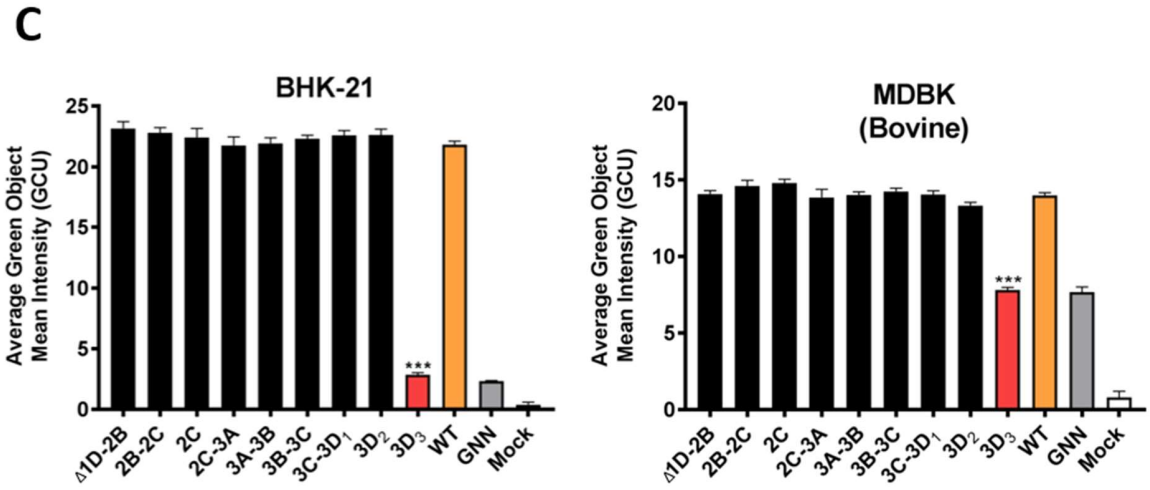

948

949 **(A)** Schematic representation of CDLR replicons. Mutated regions were firstly inserted
950 into a sub-clone encoding the non-structural proteins (nsps) of the genome (Δ1D-polyA)
951 before cloning into the WT ptGFP-replicon using the unique restriction enzymes shown.
952 **(B)** CDLR replicon insert sizes and number of mutations within each region. Regions
953 were chosen based on restriction site usage within the regions encoding nsps.
954 Mutations were introduced as described within the materials and methods section. **(C)**
955 IncuCyte data represent the average cell (green object) GFP intensity per well at 8 h
956 post-transfection. Results are the mean of three independent experiments ± standard
957 error. Significant differences between WT ptGFP and CDLR replicons were determined
958 (***, $P < 0.001$). The replication-incompetent $3D^{pol}$ active site mutant (GDD → GNN)
959 ptGFP-$3D^{pol}$GNN was used as a negative control.

960

961 **Figure 4**

962 Schematic representation of predicted conserved RNA structures located at the 3'

963 terminal end of the region encoding 3D^{pol}

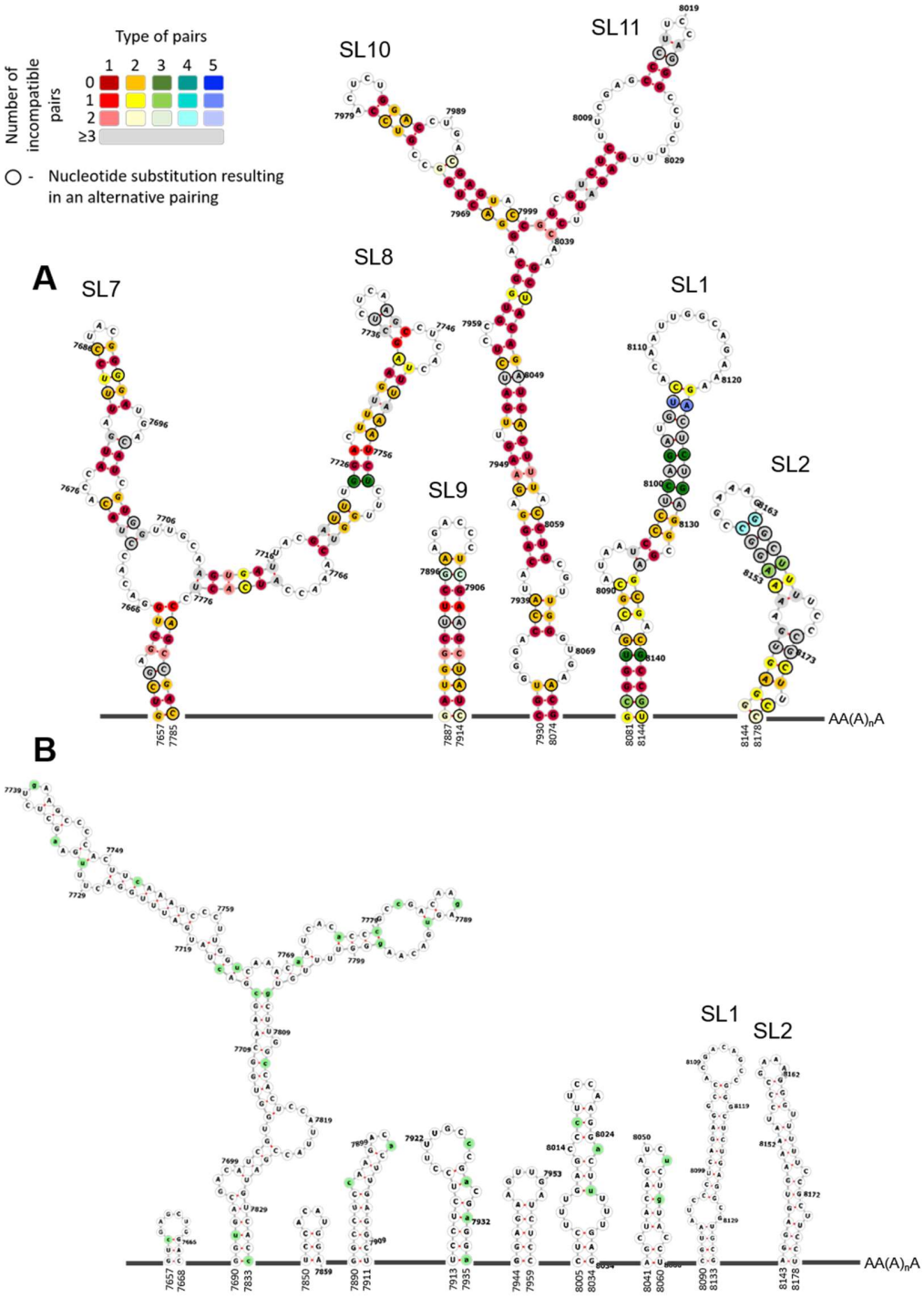

964

965 **(A)** Schematic representation of conserved (in all FMDV serotypes) RNA secondary
966 structures located at the 3' terminal end of the region encoding $3D^{pol}$ (i.e., the $3D_3$ region
967 described in Fig. 3). Conserved putative stem-loops (SL7 – SL11) are shown, where two
968 stem-loops located in the 3' UTR described before (SL1 and SL2) act as a control of the
969 computational prediction. Nucleotide positions which form conserved pairing were
970 colour-coded according to number of pairing types ('red = 1' to 'blue = 5') and
971 conservation of a pairing ('dark shades = nucleotide pairing occurred in all FMDV
972 isolates' to 'light shades = lack of nucleotide pairing in two FMDV isolates'). Positions
973 coloured in light grey show lack of pairing for three or more FMDV isolates. Black
974 circular outline indicates nucleotide position where a substitution resulted in an
975 alternative pairing (see included legend for detail). Unstructured regions are
976 represented as dark grey lines and are not drawn to scale. Numbers represent
977 nucleotide positions corresponding to the sequence of A/Brazil/1979 isolate (GenBank
978 accession number AY593788). Supplementary Table S1 specifies details represented
979 graphically in the figure legend. **(B)** Schematic representation of RNA secondary
980 structures located in the $3D_3$ region after scrambling using the CDLR algorithm,
981 demonstrating how RNA secondary structure in this region was changed. Mutated
982 nucleotide positions are highlighted in green. Unstructured regions are represented as
983 dark grey lines and are not drawn to scale. Numbers represent nucleotide positions
984 corresponding to the sequence of the A/Brazil/1979 isolate.

985

Figure 5

Extent of nucleotide conservation within hairpin loops of SL7 - SL11 RNA structures

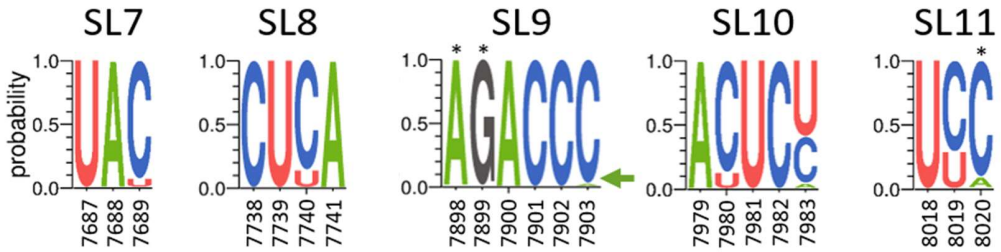

Sequence logos were generated using WebLogo 3.7.4 web server based on sequences of 118 FMDV isolates. Probability shows the extent of nucleotide occurrence at a given position. Numbers represent nucleotide positions corresponding to the sequence of A/Brazil/1979 isolate (GenBank accession number AY593788). Asterix (*) marks positions where substitution occurs in 1 out of 118 FMDV isolates but due to a limited resolution of the y axis it does not appear in the sequence logos (these are: A7898G, G7899A and C8020G). The green arrow points to C7903A substitution which due to height of the A symbol could go unnoticed.

998 **Figure 6**

999 Disruption of the predicted RNA secondary structures by silent mutagenesis

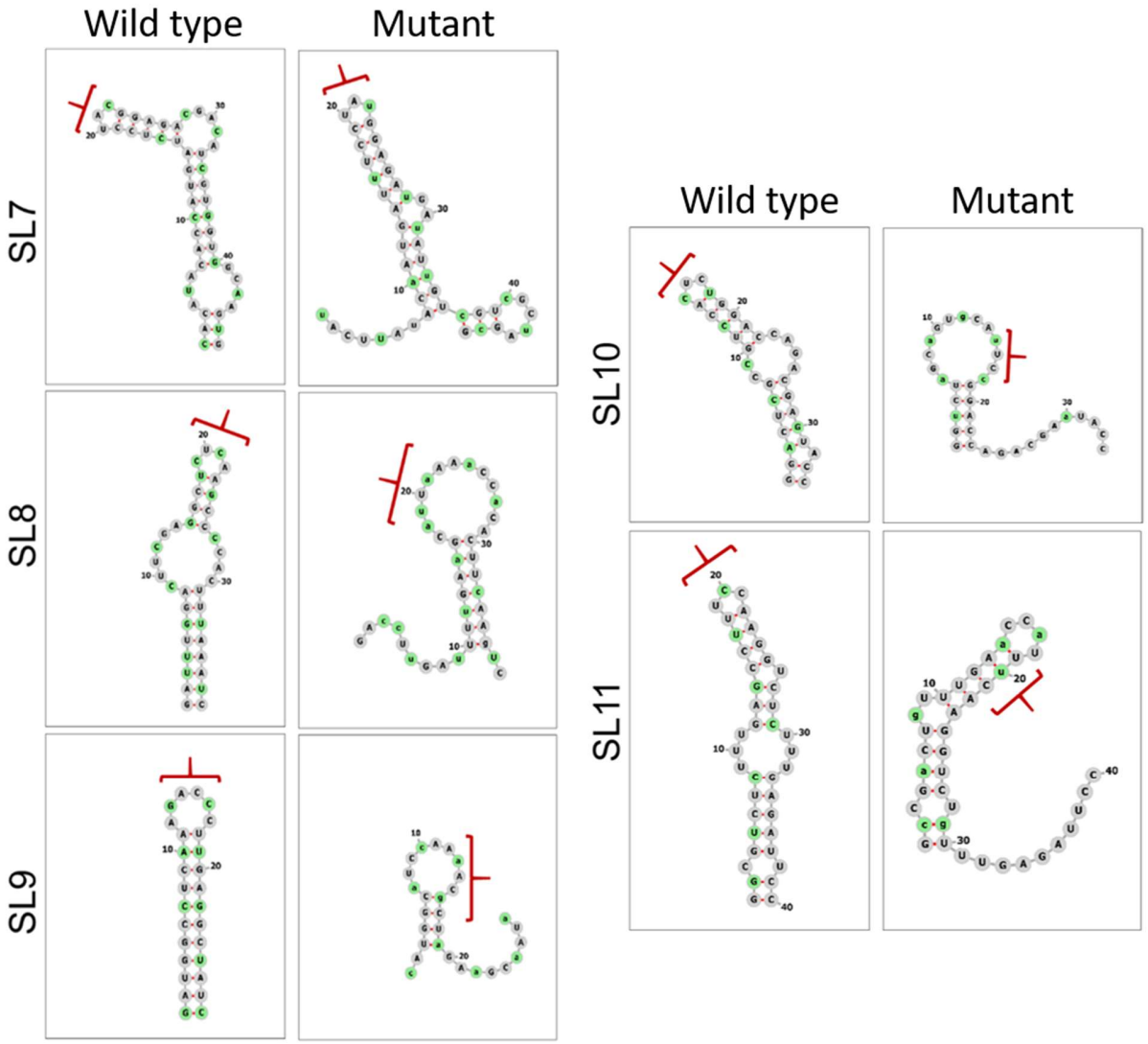

1000

1001 The conserved stem-loops identified in the 3' terminal end of the region encoding $3D^{pol}$
1002 (i.e., $3D_3$) of FMDV were predicted individually by Mfold for the WT ptGFP-replicon.
1003 Predicted WT stem-loops were mutated to cause the highest possible disruption or
1004 change to the RNA structure without affecting neighbouring stem-loops, while keeping

1005 the same amino acid sequence and dinucleotide ratio (i.e., CpG and UpA). Predicted
1006 WT and mutated stem-loops visualised in Forna web server are shown. Nucleotides
1007 highlighted in green represent mutated positions, while red brackets represent positions
1008 of the hairpin loop in the WT structures and their altered position in the disrupted
1009 structures after mutagenesis.

1010

1011 **Figure 7**

1012 Effect of individual stem-loop (SL7 - SL11) mutagenesis on replication of the FMDV

1013 replicon

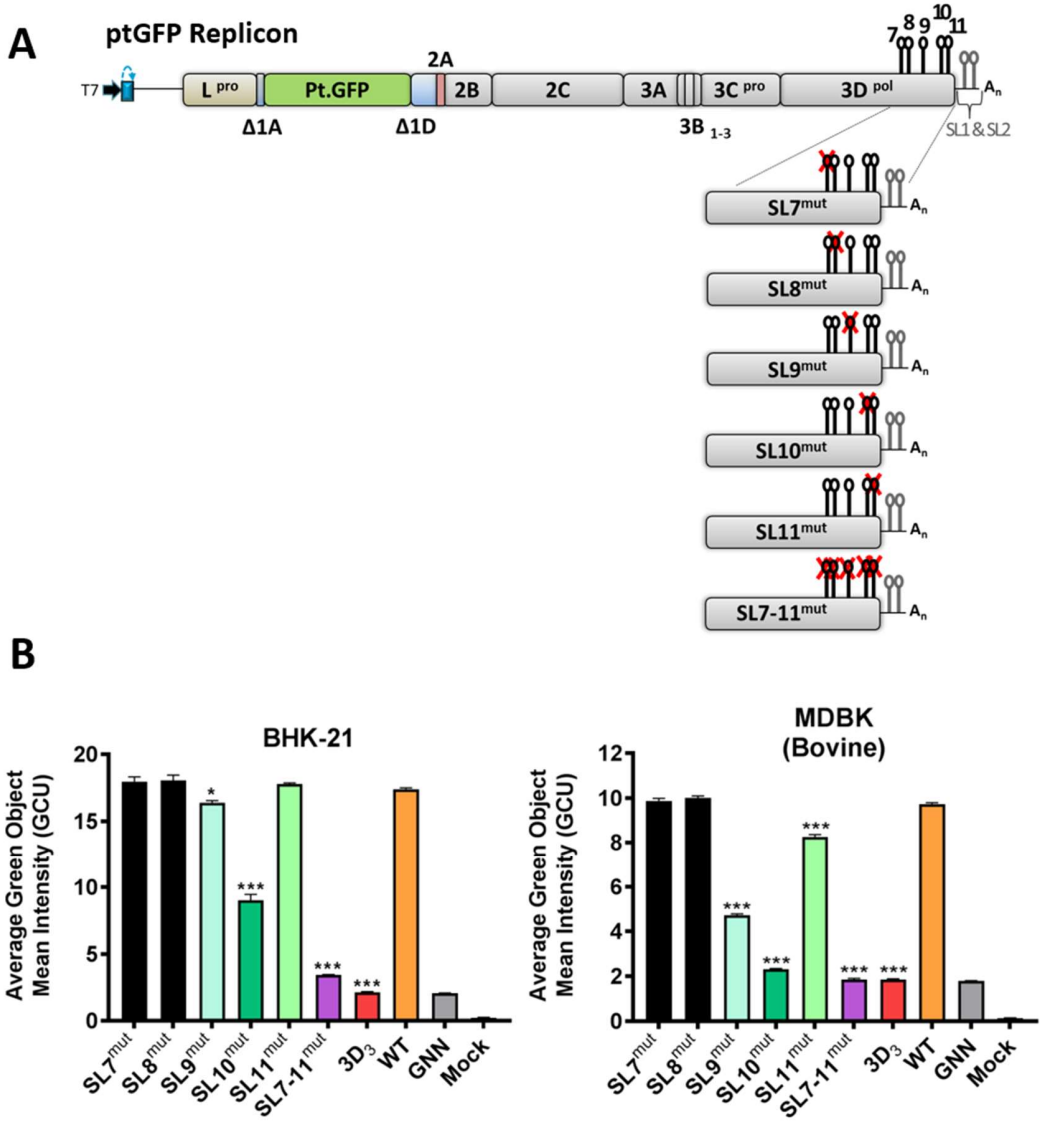

(A) Schematic representation of FMDV replicon constructs containing stem-loop mutations ($SL9^{mut}$ – $SL11^{mut}$). Sequence inserts containing stem-loop mutations were cloned directly into the ptGFP-replicon using the unique restriction enzymes BamHI and BspEI. **(B)** IncuCyte data represent the average cell (green object) GFP intensity per well at 8 h post-transfection within BHK-21 and MDBK cells. Results are the mean of three independent experiments ± standard error. Significant differences between WT ptGFP and SL^{mut} replicons were determined (*, $P < 0.05$; ***, $P < 0.001$).

1022 **Figure 8**

1023 Effect of combined mutagenesis of stem-loops 9, 10 and 11 on replication of the FMDV

1024 replicon

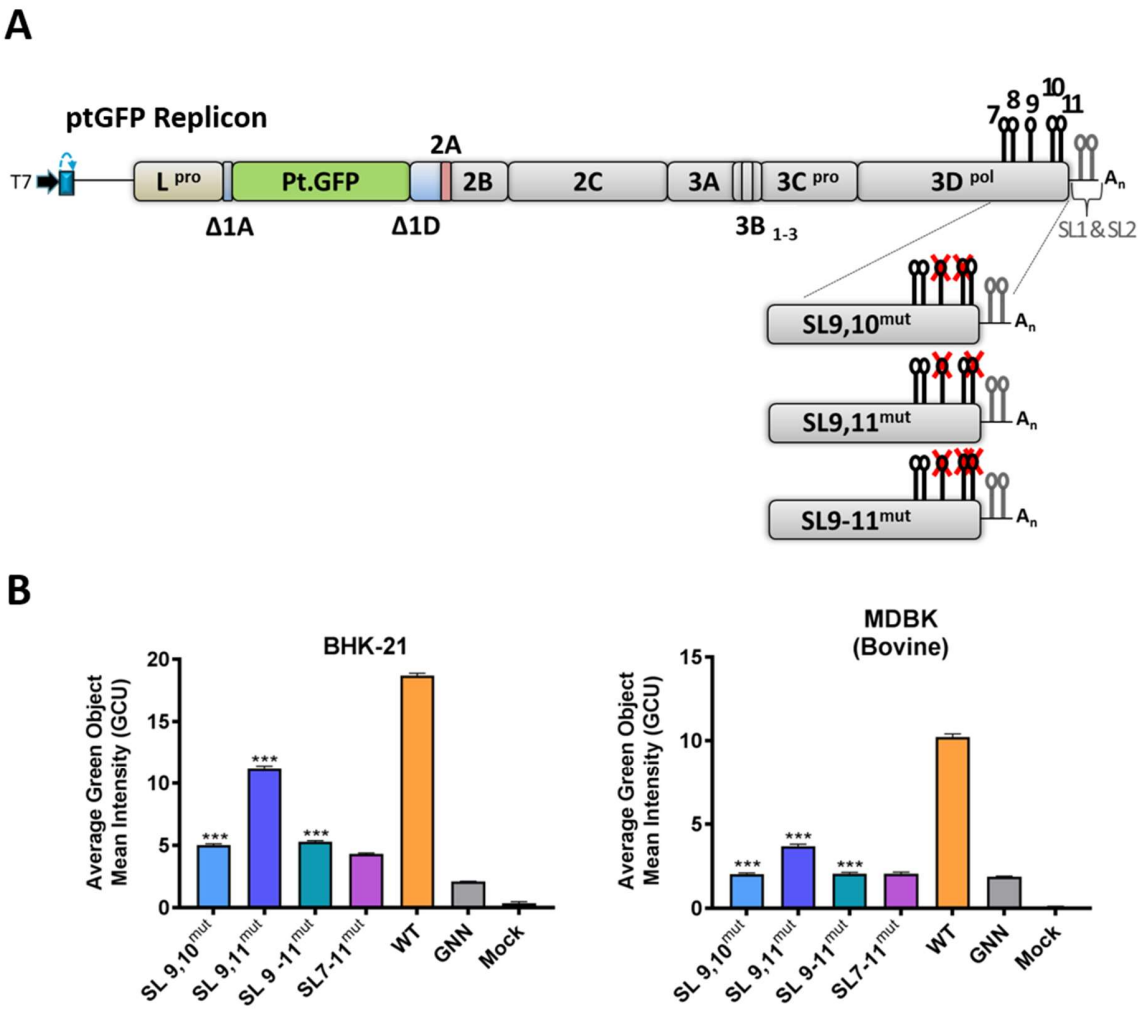

(A) Schematic representation of FMDV replicon constructs containing combined stem-loop mutations (SL9,10^{mut}, SL9,11^{mut} and SL9-11^{mut}). Sequence inserts containing stem-loop mutations were cloned directly into the ptGFP-replicon using the unique restriction enzymes BamHI and BspEI. **(B)** IncuCyte data represent the average cell (green object) GFP intensity per well at 8 h post-transfection. Results are the mean of three independent experiments ± standard error. Significant differences between WT ptGFP and SL^{mut} replicons were determined (***, $P < 0.001$).